Journal of Power Sources 394 (2018) 86–93

Contents lists available at ScienceDirect

Journal of Power Sources

journal homepage: www.elsevier.com/locate/jpowsour

Performance investigation of a micro-tubular flame-assisted fuel cell stack with 3,000 rapid thermal cycles

Ryan J. Milcarek*, Michael J. Garrett, Thomas S. Welles, Jeongmin Ahn

Department of Mechanical and Aerospace Engineering, Syracuse University, Syracuse, NY 13244-1240, USA

HIGHLIGHTS

- A novel concept for micro-combined heat and power is proposed.
- Micro-tubular flame-assisted fuel cells are tested during 3000 thermal cycles.
- Maximum heating rate of 966 °C.min^{-1} and cooling rate of 353 °C.min^{-1} are achieved.
- Significant power density of ~257 mW cm^{-2} is achieved in combustion exhaust.
- A low voltage degradation rate is measured during the thermal cycling test.

ARTICLE INFO

Keywords:
Flame-assisted fuel cell (FFC)
Micro-tubular solid oxide fuel cell (mT-SOFC)
Two-stage burner
Rich-burn
Quick-mix
Lean-burn (RQL) combustor
Micro-combined heat and power (micro-CHP)

ABSTRACT

Solid oxide fuel cell research and development has faced challenges with slow startup, slow shutdown and a limited number of thermal cycles, which hinders the technology in areas like micro-combined heat and power. A novel micro combined heat and power system, based on a boiler/hot water heater with integrated micro-tubular flame assisted fuel cells (mT-FFCs), is proposed which requires rapid startup, shutdown and thousands of thermal cycles. A 9 cell mT-FFC stack is developed and operated in a two-stage combustor. Rapid startup and shutdown of the fuel cells is demonstrated. The first-stage combustor is ignited, turned off and re-ignited for a total of 3000 on/off, thermal cycles. A maximum heating rate of 966 °C.min^{-1} and a maximum cooling rate of 353 °C.min^{-1} is achieved while thermal cycling. Despite the presence of CO in the exhaust, the anode remains porous and crack free after ~150 h of thermal cycling testing. The mT-FFC stack continues to generate significant power, even after completing the cycling test, and a low voltage degradation rate is reported.

1. Introduction

Solid oxide fuel cells (SOFCs) are electrochemical power generation devices known, in general, for high efficiency, low emissions, high fuel flexibility, no moving parts and no noise [1–4]. While these advantages give SOFCs significant potential as a cleaner source of electricity, SOFCs are hindered by a few disadvantages. The U.S. Department of Energy has cited the main challenges as long startup time, limited number of shutdowns and corrosion and breakdown of the Balance of Plant (BoP) components at high temperature [5]. As an example of slow start-up time, a heating rate of 5 °C.min^{-1} or less has been cited in many cases for a planar SOFC [6–9] although higher rates around 50 °C.min^{-1} have been achieved with metal supported planar SOFCs [10,11]. Thermal cycling tests have been conducted to assess shutdown and startup potential, but less than 50 cycles is common in the literature for planar SOFCs and for commercial systems [12–17].

This challenge is particularly common for the dual chamber SOFC (DC-SOFC) in which the fuel and oxidant streams are physically separated [3,4]. While the DC-SOFC has advantages such as high power density and efficiency, its deployment is limited by slow startup and cycling time due to stringent sealing requirements [18]. At least three means of overcoming this challenge have been proposed including the single chamber SOFC (SC-SOFC) [19–21], the no chamber direct flame fuel cell (DFFC) [18,22–43] and the micro-tubular SOFC (mT-SOFC) [9,44–48]. The SC-SOFC, DFFC and mT-SOFC reduce the sealing constraint which allows for more rapid startup. DFFCs and mT-SOFCs have been investigated for rapid start-up, rapid shut-down and thermal cycling, but the maximum number of thermal cycles found in the literature is only 400 [44] for the papers reviewed in this study. A mT-SOFC has achieved a rapid startup of 361 °C.min^{-1}, but only 11 thermal cycles [44]. A planar DFFC has achieved a more rapid startup of 1160 °C.min^{-1}, but only 26 thermal cycles [34]. Recently, a dual

* Corresponding author.
E-mail address: rjmilcar@syr.edu (R.J. Milcarek).

https://doi.org/10.1016/j.jpowsour.2018.05.060
Received 8 February 2018; Received in revised form 27 April 2018; Accepted 14 May 2018

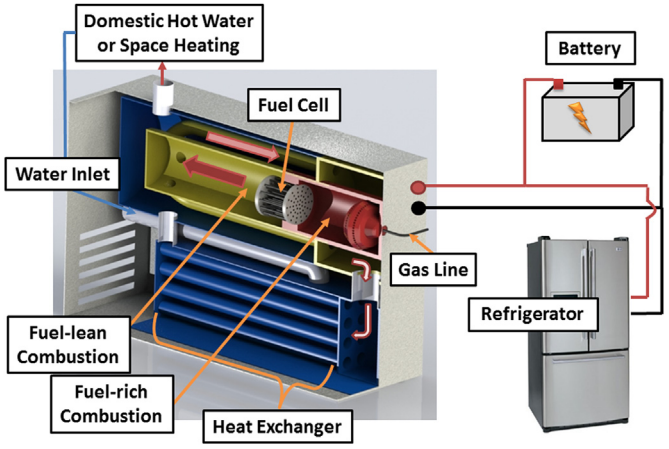

Fig. 1. One example of a FFC micro-CHP system showing a boiler with a mT-FFC stack integrated between fuel-rich and fuel-lean combustion zones.

chamber version of the original DFFC was proposed to achieve higher syngas utilization and is denoted the Flame-assisted Fuel Cell (FFC) [49–53]. To reduce the sealing constraints compared to planar and tubular SOFCs, a mT-SOFC was preferably proposed for use in the FFC setup. The combination of rapid startup capabilities while operating in combustion exhaust with a mT-SOFC is termed a micro-tubular FFC (mT-FFC) [49,50].

Combined Heat and Power (CHP) and micro-CHP systems have been proposed for the mT-FFC integrated with a residential furnace [49] and the DFFC integrated with similar systems [29,43]. Fig. 1 shows a FFC micro-CHP design integrated with a boiler. A similar integration is also possible in a furnace or hot water heater to enable a many different FFC micro-CHP systems. In this setup, a first-stage, fuel-rich combustion generates syngas and products of combustion which pass through a mT-FFC. The syngas is electrochemically converted to electricity and any remaining fuel is combusted in a second-stage, fuel-lean combustion. The heat is then recovered for hot water or space heating applications. While recent work has been conducted on fuel-rich combustion exhaust composition and FFC performance in a model fuel-rich combustion exhaust of methane and propane [49–53], a working system with actual exhaust needs further investigated. Furthermore, residential boilers startup and shutdown rapidly and can cycle over 3000 times each year [54]. A DFFC has been investigated for 26 thermal cycles only [34] while mT-FFCs have not even been investigated for thermal cycling yet. The rapid startup, shutdown and thermal cycling capabilities of a mT-FFC system need further investigation to realize the boiler shown in Fig. 1.

In this work, a mT-FFC system is developed and 9 fuel cells are connected in series to form a stack. The system is thermal cycled 3000 times and the startup and shutdown characteristics are investigated. Changes in the mT-FFC anode microstructure, stack degradation, open circuit voltage (OCV) and power density are assessed.

2. Experimental setup

2.1. Combustion chamber setup

A two-stage combustor was developed as an example of the micro-CHP system shown in Fig. 1. Fig. 2 shows the experimental setup. More details about the experimental setup are discussed in other work [55]. Methane and air (Air 2 in Fig. 2) are regulated and supplied to the fuel-rich combustion chamber via mass flow controllers. The methane flow rate is fixed at 2.4 L min^{-1} and the flow rate of air adjusts to achieve the proper equivalence ratio. The flow rates of fuel and air at different equivalence ratios are shown in Table 1. The fuel-rich combustion exhaust and mT-FFC exhaust composition was analyzed using a mass

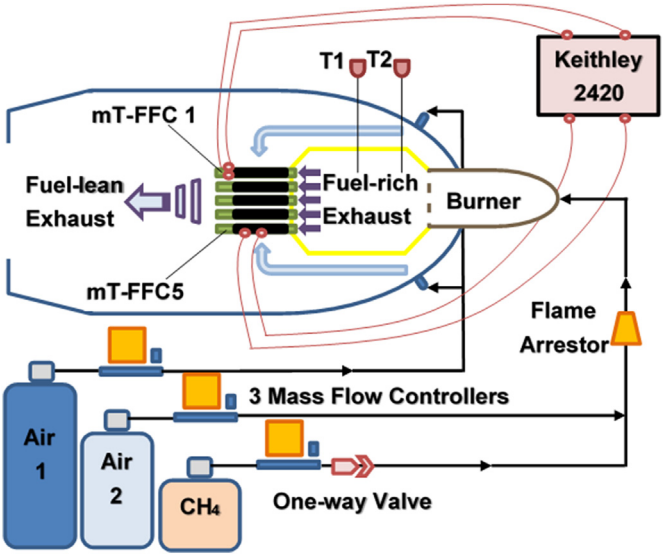

Fig. 2. Experimental setup of the mT-FFC two-stage combustion system.

Table 1
Fuel/air flow rates for the first-stage, fuel-rich combustion equivalence ratios (Ø) shown.

Equivalence ratio	Methane flow rate (mL.min^{-1})	Air flow rate (mL.min^{-1})
1.05	2400	21,760
1.10	2400	20,771
1.15	2400	19,868
1.20	2400	19,040
1.25	2400	18,278
1.30	2400	17,575
1.35	2400	16,924
1.40	2400	16,320
1.45	2400	15,757

spectrometer (MS) and gas chromatograph (GC) at different equivalence ratios. The equivalence ratio (Ø) is defined in Eq. (1). Here, n_{fuel} and n_{air} are the molar flow rates of fuel and air, respectively. The expressions n_{fuel}^{S} and n_{air}^{S} are the molar flow rates of fuel and air needed for stoichiometric reaction, respectively.

$$\varnothing = \frac{n_{fuel}/n_{air}}{n_{fuel}^{S}/n_{air}^{S}} \quad (1)$$

A spark ignitor is used to ignite the fuel/air mixture inside the fuel-rich combustion chamber. A flame-arrestor prevents flashback after ignition. Four ports distributed evenly around the experimental apparatus allow air (Air 1 in Fig. 2) to flow over the outside of the fuel-rich combustion chamber for pre-heating. Some of the oxygen is then reduced at the mT-FFC cathode for electrochemical power generation. Fuel remaining at the mT-FFC outlet is oxidized with the remaining oxygen in a fuel-lean combustion. The temperature of the flame in the fuel-rich combustion chamber (T2 in Fig. 2) and 2 cm downstream (T1 in Fig. 2) are monitored with K-type thermocouples. The mT-FFCs are arranged in a circle with the air temperature around the fuel cell at the top of the stack (mT-FFC 1 in Fig. 2) and around the fuel cell at the bottom of the stack (mT-FFC 5 in Fig. 2) monitored with K-type thermocouples. Two additional thermocouples were placed inside mT-FFC 1 and mT-FFC 5 to monitor the anode temperature during startup and cool down. The thermal cycling test was conducted with the following steps. First, the methane and air flow rate were initiated at fuel-rich conditions with a LabVIEW program. After 5s, the ignitor sparked for 5s and the fuel/air mixture ignited. The mixture reacted for 75s and then the flow rates of methane and air were stopped. The stack was allowed to cool naturally for 95s. The cycle was then repeated. The total

reaction time was chosen to achieve a relatively stable mT-FFC anode temperature above 750 °C after heating up. The length of the cool down time was chosen to achieve a mT-FFC anode temperature below 300 °C in accordance with many of the previous thermal cycling tests conducted in the literature [9,16,56].

2.2. Fuel cell fabrication and characterization

mT-SOFCs were fabricated according to a previously reported method which is not repeated here [50]. An $(La_{0.8}Sr_{0.2})_{0.95}MnO_{3-x}$ (LSM) + $(Y_2O_3)_{0.08}(ZrO_2)_{0.92}$ (YSZ) cathode was used for the 3000 thermal cycles test. The cathode was coated with silver paste for an active area of 1.66 cm^2 per fuel cell. Nine mT-SOFCs were connected together using silver wire, gold paste and ceramic paste to form a stack as discussed in previous work [51]. The stack was sealed to the fuel-rich combustion chamber using ceramic paste. The current-voltage method with four probe technique was conducted with a Keithley 2420 sourcemeter to measure the OCV, polarization and power density of the mT-FFC. The anode was assessed for carbon deposition using a scanning electron microscope (SEM) and energy dispersive x-ray spectroscopy (EDS).

3. Results and discussion

The mT-FFC stack was investigated in the experimental setup prior to conducting the thermal cycling. The polarization and power density of the mT-FFC stack at equivalence ratios from 1.05 to 1.20 were investigated. In this test, the air temperature around the cathode was 656 °C at an equivalence ratio of 1.05 and decreased to 635 °C at an equivalence ratio of 1.20. As the equivalence ratio increases, the heat release decreases and the mT-FFC temperature drops. The temperature change had a significant effect on the mT-FFC power density and peak current density. An optimal power density of ~33 mW cm^{-2} and peak current density of ~120 mA cm^{-2} was observed at an equivalence ratio of 1.05. As the equivalence ratio increased the flame temperature (measured by T2 in Fig. 2), exhaust temperature (measured by T1 in Fig. 2) and cathode temperature all decreased and resulted in high fluctuations in the mT-FFC polarization. As a result of this test, a fixed equivalence ratio of 1.05 was chosen for the thermal cycling test.

The mT-FFC stack was ignited at an equivalence ratio of 1.05 and the fuel/air flow rates were fixed for 15min. Fig. 3a shows the first polarization and power density curves obtained after 15min of testing. The peak power density was 31.9 mW cm^{-2} and the anode temperature was 800 °C. The thermal cycling program then initiated a cool down sequence which involved turning off the fuel and air flow and allowing the stack to cool for 95s prior to re-ignition. Fig. 3b shows temperature profiles obtained during 2 thermal cycles of testing. The profile denoted flame is from thermocouple T2 in Fig. 2 and the profile denoted exhaust is from thermocouple T1 in Fig. 2. The profiles denoted mT-FFC 1 and mT-FFC 5 (see Fig. 2) are from the thermocouples placed inside the two designated mT-FFCs to monitor the anode temperature. mT-FFC 1 is located at the top of the cylindrical stack and mT-FFC 5 is located at the bottom of the stack. After giving the test sufficient time to reach a steady cycling state, the temperature change of mT-FFC 5 was monitored during the heating and cooling phase. The anode temperature increased from 282 °C up to 700 °C in 25.97s for an average heating rate of 965.7 °C.min^{-1}. After reaching 700 °C the temperature increased slowly up to 752 °C over the next ~59s before cooling. The mT-FFC then cooled from 752 °C to 300 °C in 76.84s for a cooling rate of 352.9 °C.min^{-1}. Table 2 was developed to compare the thermal cycling conditions and results of this test to other thermal cycling tests conducted. As shown in Table 2, the heating rate, cooling rate and total number of thermal cycles achieved in this study are among the highest reported.

Fig. 3c shows the stack OCV variation while conducting 8 thermal cycles during the first 40 min of testing. After completing 3000 thermal cycles the methane/air flowrates were fixed for 15min and polarization and power density curves were obtained. Fig. 3d shows that the final stack OCV decreased by 0.48 V over 3000 cycles for an average degradation rate of 0.0018 V per 100 cycles per fuel cell. The results reported here are significant compared to a previous test of 50 thermal cycles which reported an average OCV degradation rate of 0.1 V per 100 cycles per fuel cell [13,62]. Another test of 10 thermal cycles reported an OCV degradation rate of 0.35 V per 100 cycles per fuel cell [7]. Fuel leakage due to sealant and electrolyte cracking and delamination of the electrodes from the electrolyte were cited as the major mechanisms for decreased OCV during thermal cycling [62,63]; however, the leakage and delamination in this setup appears to have been minimized. No noticeable leaks were developed during testing. After completing 3000 thermal cycles the power density, at an average mT-FFC voltage of 0.6 V per fuel cell, increased from 26.4 to 43.5 mW cm^{-2}. This increase in power density is partially due to a slight increase in temperature during the additional 15min of fixed fuel/air flow after thermal cycling and therefore does not reflect degradation mechanisms. The peak anode temperature was 800 °C during the initial test and increased to 826 °C during the final test. Several previous mT-SOFC thermal cycling tests of up to 400 thermal cycles have also reported an increase in power density from the beginning to the end of the testing [44]. Visual inspection of the stack showed no noticeable degradation in the cathode or interconnects after testing. Overall, the first thermal cycling test of a novel mT-FFC system found a very low OCV degradation rate and no degradation in the power density were possible after completing 3000 thermal cycles with a rapid heating and cooling rate.

After the thermal cycling test, one of the mT-FFCs was observed with a SEM and compared to a mT-FFC that had not been tested. Fig. 4a shows the Ni + YSZ anode surface before testing, which is quite porous. Fig. 4b shows the anode suface after thermal cycling. There is a noticeable difference in the amount of small scale porosity on the anode suface before and after testing. However, there are still many large pores present which formed via the pore former added to the anode during manufacturing. The decrease in porosity is partially due to the presence of carbon deposition on the anode surface. The mT-FFC concept relies on fuel-rich combustion of methane to form H_2 and CO. The CO can be broken down in the anode through the carbon disproportionation reaction according to Eq. (2) [51]. Fortunately, the reactions equilibrium constant decreases with increasing temperature [64] which makes carbon deposition less of a challenge for CO at an operating temperature around 800 °C and explains why the anode remained relatively porous despite a ~150 h test with CO present. The presence of H_2O in the exhaust also makes the water-gas shift reaction possible which helps reduce the amount of CO according to Eq. (3) [65].

$$2CO \rightarrow C + CO_2 \quad (2)$$

$$H_2O + CO \rightarrow H_2 + CO_2 \quad (3)$$

The anode cross-section was investigated further for carbon deposition. Fig. 4c shows a cross-section at the edge of the anode surface. Large pores are still present, but carbon deposition is also evident near the edge. SEM images were also obtained near the middle of the anode cross-section, which is shown in Fig. 4d. Some carbon deposition could be identified, but in general the middle of the anode cross-section showed significant porosity and little carbon deposition. As a result of the SEM investigation, carbon deposition was observed, but in general was not considered a major challenge for long-term mT-FFC operation. Furthermore, no cracks were observed on the anode surface which indicates that the mT-FFCs are durable enough to operate in a mT-FFC boiler system like the one proposed in Fig. 1 over thousands of thermal cycles.

Despite the potential for significant thermal cycling at rapid heating and cooling rates, the low power density needs improvement. The

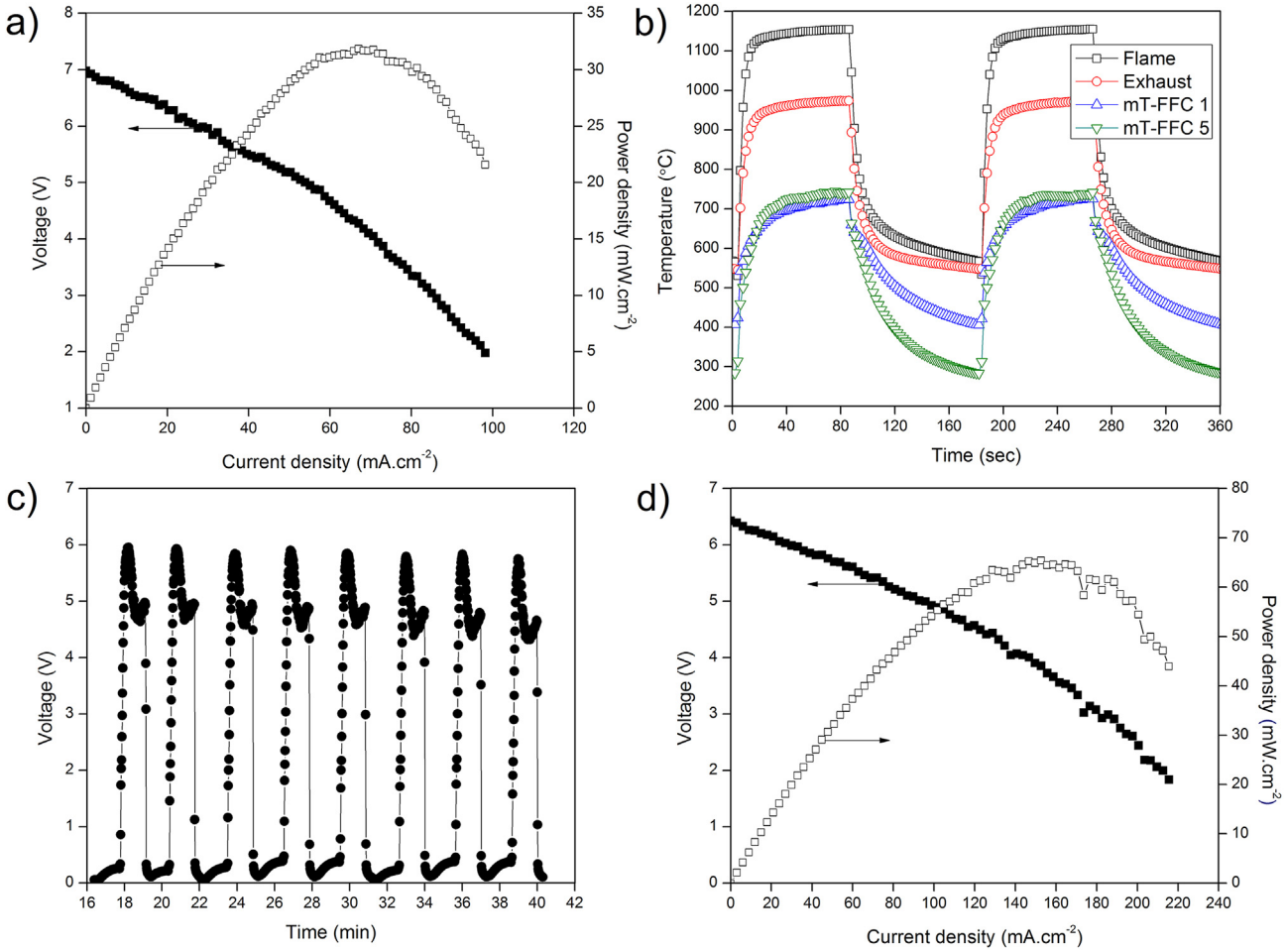

Fig. 3. 9 mT-FFC stack operating in combustion exhaust **a)** polarization and power density at an equivalence ratio of 1.05 prior to thermal cycling **b)** 2 thermal cycles of temperature data **c)** 8 thermal cycles of OCV data and **d)** polarization and power density at an equivalence ratio of 1.05 after 3000 thermal cycles.

addition of thermal insulation to the experimental setup increased the temperature of the fuel-rich and fuel-lean combustion chambers and a new mT-FFC stack with LSM + YSZ cathode was tested. The air temperature around the cathode increased significantly from 650 °C to 800 °C after improving the thermal management. Fig. 5 shows the polarization and power density results after improving the thermal management. Prior to the improvement in thermal management, the mT-FFC power density decreased as the equivalence ratio increased as discussed previously. Peak power density was observed near an equivalence ratio of 1.05. This result is due to a rapid decrease in mT-FFC temperature as the equivalence ratio increases (Ø > 1.05). After improving the thermal management, the power density increased significantly when the equivalence ratio increased due to an increase in sygnas concentration in the exhaust and more stable, high temperatures. The syngas concentration in the exhaust of the fuel-rich combustion chamber was examined at different equivalence ratios with a GC and MS. The results are shown in Table 3. As shown, the syngas concentration increases as the equivalence ratio increases. For example, at an equivalence ratio of 1.05 the H_2 concentration was 0.68% and the CO concentration was 0.04%. At an equivalence ratio of 1.30, the H_2 concentration was 4.94% and the CO concentration was 5%. The increase in syngas concentration is responsible for the increase in OCV observed in Fig. 5. This trend was predicted in previous work with a model fuel-rich combustion exhaust of methane/air at constant temperature and with theoretical calculations based on similar syngas concentrations [50,51]. The power density also increased with the syngas concentration and resulted in a decrease in concentration losses as observed in the polarization curves. As shown in Fig. 5, power densities of 96.4, 125.6, 171.1, 202.1, 230.9 and 257.1 mW cm^{-2} occurred at equivalence ratios of 1.05, 1.10, 1.15, 1.20, 1.25 and 1.30, respectively. At an equivalence ratio of 1.3 a power density of 231 mW cm^{-2} occurred at 0.6 V per fuel cell. With proper thermal management, high power density could be achieved with this setup. With a significant improvement in the mT-FFC power density and with rapid startup, rapid shutdown and 3000 thermal cycles conducted, the mT-FFC based micro-CHP system has potential to overcome some of the current challenges in SOFC system development.

From the results shown in Fig. 5, the electrical efficiency (ε) was calculated using the following equation (Eq. (4)) [22,34], where the numerator represents the electrical power generated by the mT-FFC's and the denominator represents the total chemical energy of the fuel prior to the fuel-rich combustion.

$$\varepsilon = \frac{P \cdot A \cdot V_m}{\dot{V} \cdot HHV} \tag{4}$$

P is the peak power density, A is the total mT-FFC active area, V_m is the molar volume at standard conditions (2.24×10^{-2} m^3 mol^{-1}), $\dot{V}$ is the methane flow rate (m^3. s^{-1}) at standard conditions and HHV is the higher heating value of methane (8.89×10^5 J mol^{-1}). The electrical efficiency of the final test at an equivalence ratio of 1.30 was 0.24%, which is slightly higher than a previous study on DFFCs [34]. However, the LSM based cathode is known for having much lower performance at the temperatures obtained in this study than the $Ba_{0.5}Sr_{0.5}Co_{0.8}Fe_{0.2}O_{3-x}$ (BSCF) cathode used in the previous study. A BSCF cathode may allow for much higher electrical efficiency with this setup. An upper, theoretical limit for the electrical efficiency can be calculated based on Eq.

Table 2
Literature review of thermal cycling tests conducted and their characteristics compared to the current study.

Heating rate (°C/min)	Cooling rate (°C/min)	Maximum temp. (°C)	Minimum temp. (°C)	Dwell time at max. (min)	Number of cycles	Substrate or anode, electrolyte, and cathode materials	Ref.
Planar SOFC							
1.7	N/A	1000	22	N/A	12	Ni-YSZ, PSZ, LSM-YSZ	[6]
25	3	800	100	60	40	Alumina	[57]
N/A	N/A	950	25	N/A	1	Ni-YSZ, YSZ, LSM	[58]
3	1–2	800	180	N/A	10	Ni-YSZ, YSZ, LSM	[7]
N/A	N/A	750	< 200	N/A	50	Ni-YSZ, YSZ, NA	[13]
50	50	800	200	N/A	50	Ni-YSZ, YSZ, LSCF	[10]
N/A	N/A	900	22	N/A	10	Ni-YSZ, YSZ, LSM	[14]
5	5	800	22	N/A	300	YSZ	[8]
N/A	N/A	800	250	N/A	9	LSM, LSMC, LMC, YCM	[15]
10	1	900	300	N/A	1	N/A	[16]
2	1–2	800–950	300	N/A	1	N/A	[9]
30	30	800	23	1440	13	Ni-YSZ, YSZ, LSM-YSZ	[17]
7	7	600	400	N/A	50	Ni-YSZ, YSZ, GDC, LSC	[59]
~20	N/A	850	25	~60	5	Ni-YSZ, YSZ, LSM	[27]
1160	N/A	680	100	N/A	26	Ni-SDC, SDC, BSCF-SDC	[34]
N/A	N/A	770	400	N/A	2	Ni-YSZ, YSZ, LSM-YSZ	[60]
40	20	550	150	N/A	50	Ni-YSZ, YSZ, LSC	[11]
micro-Tubular SOFC							
200	N/A	800	300	N/A	50	N/A	[9]
150	N/A	800	300	N/A	17	N/A	[9]
361	553	850	200	< 2	11	N/A, YSZ, N/A	[44]
50	N/A	800	200	N/A	400	N/A, YSZ, N/A	[44]
40	N/A	850	N/A	N/A	N/A	N/A	[45]
10	30	800	400	30	100	Ni-YSZ, YSZ, LSM-YSZ	[46]
100	100	750	400	N/A	56	Ni-YSZ, YSZ, LSM	[47]
83.3	27.8	400	150	0	5	Ni-GDC, GDC, LSCF-GDC	[61]
25	N/A	700	300	30	100	Ni-YSZ, YSZ, SDC, LSCF	[56]
966	353	753	282	1	3000	Ni-YSZ,YSZ,LSM-YSZ	[a]

Notes: Partially stabilized zirconia (PSZ) – 3 mol% Y_2O_3 + 97 mol% ZrO_2, $La_{0.8}Sr_{0.2}Mn_{0.5}Co_{0.5}O_3$ (LSMC), $LaMn_{0.4}Co_{0.6}O_3$ (LMC), $Y_{0.3}Ca_{0.7}MnO_3$ (YCM), $La_{0.6}Sr_{0.4}CoO_{3-x}$ (LSC), $Sm_{0.2}Ce_{0.8}O_{2-x}$ (SDC), $Gd_{0.2}Ce_{0.8}O_{2-x}$ (GDC), $Ba_{0.5}Sr_{0.5}Co_{0.8}Fe_{0.2}O_{3-x}$ (BSCF), $La_{0.6}Sr_{0.4}Co_{0.2}Fe_{0.8}O_{3-x}$ (LSCF).
[a] - Current study.

(5). In this case, the numerator is the reversible cell potential of the mT-FFC and it can be calculated based on complete conversion of the syngas in the exhaust to CO_2 and H_2O. At an equivalence ratio of 1.3, that is complete electrochemical conversion of 4.94% H_2 and 5% CO in the exhaust. The denominator of Eq. (5) represents the maximum chemical energy of CH_4. The change in Gibbs free energy and enthalpy can be calculated based on tabulated values available in another reference [66]. The number of moles of electrons per mole of syngas ($n_{e,syngas}$) and number of moles of electrons per mole of CH_4 fuel ($n_{e,fuel}$) are needed for this calculation. In Eq. (5), F is the Faraday constant.

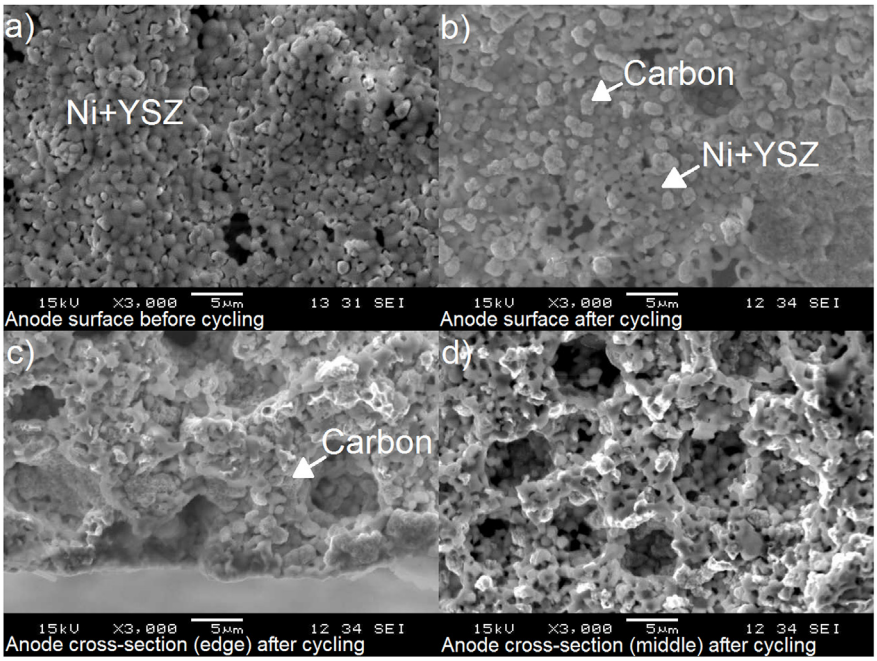

Fig. 4. SEM images of the **a)** mT-FFC anode before thermal cycling, **b)** mT-FFC anode after thermal cycling, **c)** edge of the mT-FFC anode cross-section after thermal cycling and **d)** middle of the mT-FFC anode cross-section after thermal cycling.

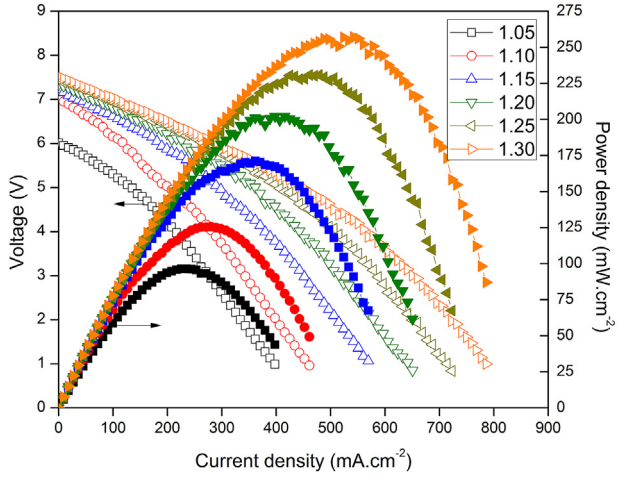

Fig. 5. mT-FFC stack polarization and power density after improving the thermal management with an LSM + YSZ cathode at equivalence ratios of 1.05, 1.10, 1.15, 1.20, 1.25 and 1.30.

Table 3
Combustion exhaust species at different equivalence ratios (Ø).

Equivalence ratio	H_2 (mol %)	CO (mol %)	CO_2 (mol %)	CH_4 (mol %)	O_2 (mol %)
1.05	0.68	0.04	11.1	0	0.90
1.10	1.49	0.12	11.8	0	0.12
1.15	2.22	1.42	11.2	0	0.11
1.20	2.94	2.29	10.2	0	0.10
1.25	4.05	3.97	9.4	0	0.09
1.30	4.94	5.00	8.8	0	0.08

Based on this calculation a maximum theoretical electrical efficiency of 9.6% results at an equivalence ratio of 1.3. Based on this analysis, further improvements in the electrical efficiency are possible.

$$\varepsilon = \frac{V}{V_{th}} = \frac{-\Delta g_{syngas}/n_{e,syngas}F}{-\Delta h_{fuel}/n_{e,fuel}F} = \frac{n_{e,fuel}}{n_{e,syngas}}\frac{\Delta g_{syngas}}{\Delta h_{fuel}} \quad (5)$$

After assessing the overall system electrical efficiency, the mT-FFC efficiency was examined more closely. To increase the mT-FFC electrical efficiency the methane flow rate was lowered and the active area was increased compared to the previous test because lower flow rate and higher active area are expected to improve the utilization of the syngas. The fuel-rich equivalence ratio was set to 1.20 and methane flow rate was fixed at 1.6 L.min^{-1}. The cathode active area was increased to 2.7 cm^2 per fuel cell. The concentration of H_2 and CO upstream and downstream of the mT-FFC were analyzed with a MS and GC while the mT-FFC was loaded with a fixed current density of 200 mA cm^{-2}. At this current density, the mT-FFC stack voltage was ~0.5 V per fuel cell. The H_2 concentration in the exhaust upstream of the mT-FFC at these conditions was 2.94% and CO concentration was 2.29%. The H_2 concentration in the exhaust downstream of the mT-FFC decreased to 2.80% (4.9% of the H_2 utilized) after the fuel cell was loaded with a fixed current density of 200 mA cm^{-2}, while the CO concentration decreased to 2.27% (0.9% of the CO utilized). As a result, ~6 times more H_2 was utilized at 200 mA cm^{-2} than CO in this test. The electrochemical oxidation rate of H_2 is known to be much faster than CO [67]. From these results, it is evident that the H_2 in the exhaust has a much more significant effect on the mT-FFC performance than CO. There is an opportunity for further improvement in the mT-FFC electrical efficiency as more than 95% of the H_2 and 99% of the CO were still available in the mT-FFC exhaust. A mT-FFC with a much larger active area could have much higher fuel utilization than reported here. While the electrical efficiency still needs further improvement, the CHP system shown in Fig. 1 has a direct use for waste heat which will allow for higher total efficiency (from heat and power utilization) of the system.

To assess the actual mT-FFC efficiency, the electrical efficiency was recalculated based on the amount of H_2 and CO actually utilized at 200 mA cm^{-2} using Eq. (4). In this case, the power density, P, was 103.3 mW cm^{-2}, and the area, A, was 24.3 cm^2. The HHV of syngas was calculated as 5.6881×10^5 J mol^{-1} using tabulated thermodynamic values [66]. The total flow rate of exhaust at an equivalence ratio of 1.2 was 14,293.3 mL min^{-1}. Of the 2.9% H_2 in the exhaust (~419.8 mL min^{-1} total average H_2 flow rate generated by fuel-rich combustion), 4.9% (~20.6 mL min^{-1}) was utilized by the mT-FFC when loaded with a current density of 200 mA cm^{-2}. Similarly ~3 mL min^{-1} of CO was utilized at 200 mA cm^{-2}. The total flow rate of syngas, $\dot{V}$, was 23.5 mL min^{-1}. Based on this data obtained from the actual amount of H_2 and CO utilized, the electrical efficiency of the mT-FFC was 25%. Despite the low net electrical efficiency of the system, the mT-FFC is actually operating with reasonable efficiency based on a very limited fuel supply. Higher electrical efficiency is possible as the mT-FFCs used in this study show high ohmic resistance due to the external anode current collection [51] and have limited active area.

4. Conclusions

A mT-FFC based micro-CHP system has been proposed in this work. To assess the potential of the technology, a mT-FFC stack was developed and integrated with fuel-rich and fuel-lean combustion chambers and 3000 thermal cycles were conducted. The number of thermal cycles achieved with the mT-FFC is a significant increase over previously reported thermal cycling tests. A rapid heating rate of 965.7 °C.min^{-1} and a rapid cooling rate of 352.9 °C.min^{-1} were achieved. A mT-FFC stack with LSM + YSZ cathode showed low degradation in OCV (0.0018 V per 100 cycles per fuel cell) and no degradation in power density during the test. Initially the mT-FFC showed a peak power density around an equivalence ratio of 1.05 due to a decrease in the fuel cell temperature when the equivalence ratio exceeded 1.05. This occurred despite the increase in syngas concentration in the exhaust at higher equivalence ratios. After making improvements in the thermal management, the mT-FFC power density increased significantly as the equivalence ratio increased due to more stable high temperatures and increased syngas concentration. A reasonable power density of 231 mW cm^{-2} at 0.6 V per fuel cell at an equivalence ratio of 1.3 was achieved in this study for the mT-FFC stack. The mT-FFC fuel utilization was investigated and only ~4.9% of the H_2 and ~0.9% of the CO were actually utilized with a current density of 200 mA cm^{-2}. The mT-FFC was 25% efficient in converting this limited amount of syngas into electricity. Significant improvements are possible by optimizing the system and fuel cells to utilize more of the H_2 and CO available in the exhaust.

Acknowledgement

This material is based upon work supported by an Agreement with Syracuse University awarded by its Syracuse Center of Excellence for Environmental and Energy Systems with funding under prime award number DE-EE0006031 from the US Department of Energy and matching funding under award number 53367 from the New York State Energy Research and Development Authority (NYSERDA) and under NYSERDA contract 61736. This material is also based upon work supported by the National Science Foundation Graduate Research Fellowship Program under Grant No. 1746928.

References

[1] R. Bove, S. Ubertini, Modeling solid oxide fuel cell operation: approaches, techniques and results, J. Power Sources 159 (2006) 543–559, http://dx.doi.org/10.1016/j.jpowsour.2005.11.045.

[2] F. Zink, Y. Lu, L. Schaefer, A solid oxide fuel cell system for buildings, Energy Convers. Manag. 48 (2007) 809–818, http://dx.doi.org/10.1016/j.enconman.2006.09.010.

[3] R.J. Milcarek, K. Wang, M.J. Garrett, J. Ahn, Performance investigation of dual layer yttria-stabilized zirconia–samaria-doped ceria electrolyte for intermediate temperature solid oxide fuel cells, J. Electrochem. Energy Convers. Storage 13 (2016) 11002, http://dx.doi.org/10.1115/1.4032708.

[4] R.J. Milcarek, K. Wang, R.L. Falkenstein-Smith, J. Ahn, Performance variation with SDC buffer layer thickness, Int. J. Hydrogen Energy 41 (2016) 9500–9506, http://dx.doi.org/10.1016/j.ijhydene.2016.04.113.

[5] U.S. Department of Energy, Office of energy efficiency & renewable energy, Comparison of Fuel Cell Technologies (2016), http://energy.gov/eere/fuelcells/downloads/comparison-fuel-cell-technologies-fact-sheet , Accessed date: 8 February 2018.

[6] S. Taniguchi, M. Kadowaki, T. Yasuo, Y. Akiyama, Y. Miyake, K. Nishio, Improvement of thermal cycle characteristics of a planar-type solid oxide fuel cell by using ceramic fiber as sealing material, J. Power Sources 90 (2000) 163–169, http://dx.doi.org/10.1016/S0378-7753(00)00405-5.

[7] G. Schiller, T. Franco, M. Lang, P. Metzger, A.O. Stormer, Recent results of the SOFC APU development at DLR, in: S.C. Singhal, J. Mizusaki (Eds.), Solid Oxide Fuel Cells IX, The Electrochemical Society, Pennington, NJ, 2005, pp. 66–75.

[8] R.N. Singh, Sealing technology for solid oxide fuel cells, Int. J. Appl. Ceram. Technol. 4 (2007) 134–144, http://dx.doi.org/10.1111/j.1744-7402.2007.02128.x.

[9] W. Bujalski, C.M. Dikwal, K. Kendall, Cycling of three solid oxide fuel cell types, J. Power Sources 171 (2007) 96–100, http://dx.doi.org/10.1016/j.jpowsour.2007.01.029.

[10] Y.B. Matus, L.C. De Jonghe, C.P. Jacobson, S.J. Visco, Metal-supported solid oxide fuel cell membranes for rapid thermal cycling, Solid State Ionics 176 (2005) 443–449, http://dx.doi.org/10.1016/j.ssi.2004.09.056.

[11] K.J. Kim, B.H. Park, S.J. Kim, Y. Lee, H. Bae, G.M. Choi, Micro solid oxide fuel cell fabricated on porous stainless steel: a new strategy for enhanced thermal cycling ability, Sci. Rep. 6 (2016) 22443, http://dx.doi.org/10.1038/srep22443.

[12] Y.S. Chou, J.W. Stevenson, L.A. Chick, Ultra-low leak rate of hybrid compressive mica seals for solid oxide fuel cells, J. Power Sources 112 (2002) 130–136, http://dx.doi.org/10.1016/S0378-7753(02)00356-7.

[13] E. Tang, D. Prediger, M. Pastula, B. Borglum, The status of SOFC development at versa power systems, in: S.C. Singhal, J. Mizusaki (Eds.), Solid Oxide Fuel Cells IX, The Electrochemical Society, Pennington, NJ, 2005, pp. 89–97.

[14] A. Atkinson, B. Sun, Residual stress and thermal cycling of planar solid oxide fuel cells, Mater. Sci. Technol. 23 (2007) 1135–1143, http://dx.doi.org/10.1179/026708307X232910.

[15] E. Konysheva, J. Laatsch, E. Wessel, F. Tietz, N. Christiansen, L. Singheiser, K. Hilpert, Influence of different perovskite interlayers on the electrical conductivity between $La_{0.65}Sr_{0.3}MnO_3$ and Fe/Cr-based steels, Solid State Ionics 177 (2006) 923–930, http://dx.doi.org/10.1016/j.ssi.2006.01.046.

[16] W. Bujalski, J. Paragreen, G. Reade, S. Pyke, K. Kendall, Cycling studies of solid oxide fuel cells, J. Power Sources 157 (2006) 745–749, http://dx.doi.org/10.1016/j.jpowsour.2006.01.060.

[17] J. Van herle, D. Perednis, K. Nakamura, S. Diethelm, M. Zahid, A. Aslanides, T. Somekawa, Y. Baba, K. Horiuchi, Y. Matsuzaki, M. Yoshimoto, O. Bucheli, Ageing of anode-supported solid oxide fuel cell stacks including thermal cycling, and expansion behaviour of MgO-NiO anodes, J. Power Sources 182 (2008) 389–399, http://dx.doi.org/10.1016/j.jpowsour.2008.03.006.

[18] K. Wang, P. Zeng, J. Ahn, High performance direct flame fuel cell using a propane flame, Proc. Combust. Inst. 33 (2011) 3431–3437, http://dx.doi.org/10.1016/j.proci.2010.07.047.

[19] I. Riess, P.J. van der Put, J. Schoonman, Solid oxide fuel cells operating on uniform mixtures of fuel and air, Solid State Ionics 82 (1995) 1–4, http://dx.doi.org/10.1016/0167-2738(95)00210-W.

[20] S. Raz, M.J.G. Jak, J. Schoonman, I. Riess, Supported mixed-gas fuel cells 149 (2002) 335–341.

[21] I. Riess, On the single chamber solid oxide fuel cells, J. Power Sources 175 (2008) 325–337, http://dx.doi.org/10.1016/j.jpowsour.2007.09.041.

[22] M. Horiuchi, S. Suganuma, M. Watanabe, Electrochemical power generation directly from combustion flame of gases, liquids, and solids, J. Electrochem. Soc. 151 (2004) A1402, http://dx.doi.org/10.1149/1.1778168.

[23] H. Kronemayer, D. Barzan, M. Horiuchi, S. Suganuma, Y. Tokutake, C. Schulz, W.G. Bessler, A direct-flame solid oxide fuel cell (DFFC) operated on methane, propane, and butane, J. Power Sources 166 (2007) 120–126, http://dx.doi.org/10.1016/j.jpowsour.2006.12.074.

[24] M. Vogler, D. Barzan, H. Kronemayer, C. Schulz, M. Horiuchi, S. Suganuma, Y. Tokutake, J. Warnatz, W.G. Bessler, Direct-flame solid-oxide fuel cell (DFFC): a thermally self-sustained, air self- breathing, hydrocarbon-operated SOFC system in a simple, No-Chamber setup, ECS Trans., ECS (2007) 555–564, http://dx.doi.org/10.1149/1.2729136.

[25] M. Vogler, M. Horiuchi, W.G. Bessler, Modeling, simulation and optimization of a no-chamber solid oxide fuel cell operated with a flat-flame burner, J. Power Sources 195 (2010) 7067–7077, http://dx.doi.org/10.1016/j.jpowsour.2010.04.030.

[26] M.M. Hossain, J. Myung, R. Lan, M. Cassidy, I. Burns, S. Tao, J.T.S. Irvine, Study on direct flame solid oxide fuel cell using flat burner and ethylene flame, ECS Trans. 68 (2015) 1989–1999, http://dx.doi.org/10.1149/06801.1989ecst.

[27] X. Zhu, B. Wei, Z. Lü, L. Yang, X. Huang, Y. Zhang, M. Liu, A direct flame solid oxide fuel cell for potential combined heat and power generation, Int. J. Hydrogen Energy 37 (2012) 8621–8629, http://dx.doi.org/10.1016/j.ijhydene.2012.02.161.

[28] Y. Wang, L. Sun, L. Luo, Y. Wu, L. Liu, J. Shi, The study of portable direct-flame solid oxide fuel cell (DF-SOFC) stack with butane fuel, J. Fuel Chem. Technol. 42 (2014) 1135–1139, http://dx.doi.org/10.1016/S1872-5813(14)60045-1.

[29] Y. Wang, Y. Shi, M. Ni, N. Cai, A micro tri-generation system based on direct flame fuel cells for residential applications, Int. J. Hydrogen Energy 39 (2014) 5996–6005, http://dx.doi.org/10.1016/j.ijhydene.2014.01.183.

[30] S. Endo, Y. Nakamura, Power generation properties of direct flame fuel cell (DFFC), J. Phys. Conf. Ser 557 (2014) 12119, http://dx.doi.org/10.1088/1742-6596/557/1/012119.

[31] K. Wang, R. Ran, Y. Hao, Z. Shao, W. Jin, N. Xu, A high-performance no-chamber fuel cell operated on ethanol flame, J. Power Sources 177 (2008) 33–39, http://dx.doi.org/10.1016/j.jpowsour.2007.11.004.

[32] Y. Wang, Y. Shi, X. Yu, N. Cai, J. Qian, S. Wang, Experimental characterization of a direct methane flame solid oxide fuel cell power generation unit, J. Electrochem. Soc. 161 (2014) F1348–F1353, http://dx.doi.org/10.1149/2.0381414jes.

[33] Y. Wang, Y. Shi, X. Yu, N. Cai, Thermal shock resistance and failure probability analysis on solid oxide electrolyte direct flame fuel cells, J. Power Sources 255 (2014) 377–386, http://dx.doi.org/10.1016/j.jpowsour.2014.01.035.

[34] K. Wang, R.J. Milcarek, P. Zeng, J. Ahn, Flame-assisted fuel cells running methane, Int. J. Hydrogen Energy 40 (2015), http://dx.doi.org/10.1016/j.ijhydene.2015.01.128.

[35] X. Zhu, Z. Lü, B. Wei, X. Huang, Z. Wang, W. Su, Direct flame SOFCs with $La_{0.75}Sr_{0.25}Cr_{0.5}Mn_{0.5}O_{3-\delta}$/Ni coimpregnated yttria-stabilized zirconia anodes operated on liquefied petroleum gas flame, J. Electrochem. Soc. 157 (2010) B1838, http://dx.doi.org/10.1149/1.3500976.

[36] Y.Q. Wang, Y.X. Shi, X.K. Yu, N.S. Cai, S.Q. Li, Integration of solid oxide fuel cells with multi-element diffusion flame burners, J. Electrochem. Soc. 160 (2013) F1241–F1244, http://dx.doi.org/10.1149/2.051311jes.

[37] T. Hirasawa, S. Kato, A study on energy conversion efficiency of direct flame fuel cell supported by clustered diffusion microflames, J. Phys. Conf. Ser 557 (2014) 12120, http://dx.doi.org/10.1088/1742-6596/557/1/012120.

[38] Y. Wang, Y. Shi, N. Cai, X. Ye, S. Wang, Performance characteristics of a micro-tubular solid oxide fuel cell operated with a fuel-rich methane flame, ECS Trans. 68 (2015) 2237–2243, http://dx.doi.org/10.1149/06801.2237ecst.

[39] Y. Nakamura, S. Endo, Power generation performance of direct flame fuel cell (DFFC) impinged by small jet flames, J. Micromech. Microeng. 25 (2015) 104015, http://dx.doi.org/10.1088/0960-1317/25/10/104015.

[40] Y. Wang, H. Zeng, T. Cao, Y. Shi, N. Cai, X. Ye, S. Wang, Start-up and operation characteristics of a flame fuel cell unit, Appl. Energy 178 (2016) 415–421, http://dx.doi.org/10.1016/j.apenergy.2016.06.067.

[41] Y. Wang, H. Zeng, Y. Shi, T. Cao, N. Cai, X. Ye, S. Wang, Power and heat co-generation by micro-tubular flame fuel cell on a porous media burner, Energy 109 (2016) 117–123, http://dx.doi.org/10.1016/j.energy.2016.04.095.

[42] M.C. Tucker, A.S. Ying, Metal-supported solid oxide fuel cells operated in direct-flame configuration, Int. J. Hydrogen Energy 42 (2017) 24426–24434, http://dx.doi.org/10.1016/j.ijhydene.2017.07.224.

[43] H. Zeng, Y. Wang, Y. Shi, N. Cai, Biogas-fueled flame fuel cell for micro-combined heat and power system, Energy Convers. Manag. 148 (2017) 701–707, http://dx.doi.org/10.1016/j.enconman.2017.06.039.

[44] Y. Du, C. Finnerty, J. Jiang, Thermal stability of portable microtubular SOFCs and stacks, J. Electrochem. Soc. 155 (2008) B972, http://dx.doi.org/10.1149/1.2953590.

[45] V. Lawlor, S. Griesser, G. Buchinger, A.G. Olabi, S. Cordiner, D. Meissner, Review of the micro-tubular solid oxide fuel cell. Part I. Stack design issues and research activities, J. Power Sources 193 (2009) 387–399, http://dx.doi.org/10.1016/j.jpowsour.2009.02.085.

[46] A.R. Hanifi, A. Torabi, M. Zazulak, T.H. Etsell, L. Yamarte, P. Sarkar, M. Tucker, Improved redox and thermal cycling resistant tubular ceramic fuel cells, ECS Trans. 35 (2011) 409–418, http://dx.doi.org/10.1149/1.3570016.

[47] K.S. Howe, A.R. Hanifi, K. Kendall, M. Zazulak, T.H. Etsell, P. Sarkar, Performance of microtubular SOFCs with infiltrated electrodes under thermal cycling, Int. J. Hydrogen Energy 38 (2013) 1058–1067, http://dx.doi.org/10.1016/j.ijhydene.2012.10.098.

[48] K. Kendall, Progress in microtubular solid oxide fuel cells, Int. J. Appl. Ceram. Technol. 7 (2010) 1–9, http://dx.doi.org/10.1111/j.1744-7402.2008.02350.x.

[49] R.J. Milcarek, K. Wang, R.L. Falkenstein-Smith, J. Ahn, Micro-tubular flame-assisted fuel cells for micro-combined heat and power systems, J. Power Sources 306 (2016) 148–151, http://dx.doi.org/10.1016/j.jpowsour.2015.12.018.

[50] R.J. Milcarek, M.J. Garrett, K. Wang, J. Ahn, Micro-tubular flame-assisted fuel cells running methane, Int. J. Hydrogen Energy 41 (2016), http://dx.doi.org/10.1016/j.ijhydene.2016.08.155.

[51] R.J. Milcarek, M.J. Garrett, J. Ahn, Micro-tubular flame-assisted fuel cell stacks, Int. J. Hydrogen Energy 41 (2016) 21489–21496, http://dx.doi.org/10.1016/j.ijhydene.2016.09.005.

[52] R.J. Milcarek, M.J. Garrett, A. Baskaran, J. Ahn, Combustion characterization and model fuel development for micro-tubular flame-assisted fuel cells, JoVE (2016), http://dx.doi.org/10.3791/54638 e54638.

[53] R.J. Milcarek, M.J. Garrett, J. Ahn, Micro-tubular flame-assisted fuel cells, J. Fluid Sci. Technol. 12 (2017), http://dx.doi.org/10.1299/jfst.2017jfst0021 JFST0021-JFST0021.

[54] L. Arena, O. Faakye, Optimizing Hydronic System Performance in Residential Applications, (2013), http://dx.doi.org/10.2172/1096690.

[55] R.J. Milcarek, J. Ahn, Rich-burn, flame-assisted fuel cell, quick-mix, lean-burn (RFQL) combustor and power generation, J. Power Sources 381 (2018) 18–25, http://dx.doi.org/10.1016/j.jpowsour.2018.02.006.

[56] M. Torrell, A. Morata, P. Kayser, M. Kendall, K. Kendall, A. Tarancón, Performance and long term degradation of 7 W micro-tubular solid oxide fuel cells for portable

applications, J. Power Sources 285 (2015) 439–448, http://dx.doi.org/10.1016/j.jpowsour.2015.03.030.
[57] Y.-S. Chou, J.W. Stevenson, Thermal cycling of advanced compressive seals for solid oxide fuel cells, J. Power Sources 112 (2002) 376–383, http://dx.doi.org/10.1016/S0378-7753(02)00444-5.
[58] A.C. Müller, D. Herbstritt, E. Ivers-Tiffée, Development of a multilayer anode for solid oxide fuel cells, Solid State Ionics 152–153 (2002) 537–542, http://dx.doi.org/10.1016/S0167-2738(02)00357-0.
[59] H.S. Noh, K.J. Yoon, B.K. Kim, H.J. Je, H.W. Lee, J.H. Lee, J.W. Son, Thermo-mechanical stability of multi-scale-architectured thin-film-based solid oxide fuel cells assessed by thermal cycling tests, J. Power Sources 249 (2014) 125–130, http://dx.doi.org/10.1016/j.jpowsour.2013.10.101.
[60] A. Hagen, J.V.T. Høgh, R. Barfod, Accelerated testing of solid oxide fuel cell stacks for micro combined heat and power application, J. Power Sources 300 (2015) 223–228, http://dx.doi.org/10.1016/j.jpowsour.2015.09.054.
[61] T. Suzuki, Y. Funahashi, T. Yamaguchi, Y. Fujishiro, M. Awano, Cube-type micro SOFC stacks using sub-millimeter tubular SOFCs, J. Power Sources 183 (2008) 544–550, http://dx.doi.org/10.1016/j.jpowsour.2008.05.026.
[62] L. Liu, G.-Y. Kim, A. Chandra, Modeling of thermal stresses and lifetime prediction of planar solid oxide fuel cell under thermal cycling conditions, J. Power Sources 195 (2010) 2310–2318 https://doi.org/10.1016/j.jpowsour.2009.10.064.
[63] N. Hart, Scale-up of the IP-sofc to Multi-kilowatt Levels F/01/00197/REP URN 04/556, (2004).
[64] T. Kim, S. Moon, S.-I. Hong, Internal carbon dioxide reforming by methane over Ni-YSZ-CeO_2 catalyst electrode in electrochemical cell, Appl. Catal. Gen. 224 (2002) 111–120 https://doi.org/10.1016/S0926-860X(01)00735-9.
[65] H. Alqahtany, D. Eng, M. Stoukides, Methane steam reforming over Fe electrodes in a solid electrolyte cell, Energy Fuels 7 (1993) 495–504, http://dx.doi.org/10.1021/ef00040a010.
[66] R. O'Hayre, S. Cha, W. Colella, F.B. Prinz, Fuel Cell Fundamentals, Second, Wiley, New York, 2009.
[67] Y. Matsuzaki, I. Yasuda, Electrochemical oxidation of H_2 and CO in a H_2-H_2O-CO-CO_2 system at the interface of a Ni-YSZ cermet electrode and YSZ electrolyte, J. Electrochem. Soc. 147 (2000) 1630, http://dx.doi.org/10.1149/1.1393409.

Glossary

A: Total fuel cell active area
BoP: Balance of Plant
BSCF: $Ba_{0.5}Sr_{0.5}Co_{0.8}Fe_{0.2}O_{3-x}$
CHP: Combined heat and power
DC-SOFC: Dual chamber solid oxide fuel cell
DFFC: Direct flame fuel cell
EDS: Energy dispersive x-ray spectroscopy
F: Faraday constant
FFC: Flame-assisted fuel cell
GC: Gas chromatograph
HHV: Higher heating value
LSM: Lanthanum strontium manganite, $(La_{0.8}Sr_{0.2})_{0.95}MnO_{3-x}$
MS: Mass spectrometer
mT-FFC: micro-tubular flame-assisted fuel cell
mT-SOFC: micro-tubular solid oxide fuel cell
$n_{e,fuel}$: Number of moles of electrons per mole of fuel
$n_{e,syngas}$: Number of moles of electrons per mole of syngas
n_{fuel}: Molar flow rate of fuel
n_{air}: Molar flow rate of air
n_{fuel}^{S}: Molar flow rate of fuel for stoichiometric reaction
n_{air}^{S}: Molar flow rate of air for stoichiometric reaction
OCV: Open circuit voltage
P: Peak power density
SC-SOFC: Single chamber solid oxide fuel cell
SEM: Scanning electron microscope
SOFC: Solid oxide fuel cell
V: Reversible cell potential
V_m: Molar volume at standard conditions
V_{th}: Thermoneutral voltage
$\dot{V}$: Methane flow rate at standard conditions
YSZ: Yttria stabilized zirconia, $(Y_2O_3)_{0.08}(ZrO_2)_{0.92}$
E: mT-FFC electrical efficiency
Ø: Equivalence ratio
Δg: Change in Gibbs free energy
Δh: Change in enthalpy